Elastic and Inelastic Low-Energy-Electron Diffraction From Al(100). II. Absolute-Intensity Measurements*

J. M. Burkstrand†

Coordinated Science Laboratory and Department of Physics, University of Illinois, Urbana, Illinois 61801

(Received 3 May 1972; revised manuscript received 10 October 1972)

Elastic and inelastic low-energy-electron-diffraction (ELEED, ILEED) observation have been made on a clean (100) surface of Al. Measurements on the (10) and (11) elastic-diffraction beams were made using normally incident electrons in the energy range $30 \leq E \leq 170$ eV. Peaks in the energy-loss distribution are seen near 5, 10, 15, 26, and 31 eV, the dominant peaks near 10 and 15 eV corresponding to surface- and bulk-plasmon excitations, respectively. Two types of structure are observed in the inelastic angular profiles: one closely correlated with the structure in the elastic angular profile and the second being substructure corresponding to different ILEED conditions. Absolute intensities of the energy-intensity profiles (as a function of incident energy) for the (10) and (11) elastic and inelastic diffraction beams have been measured. These profiles also show primary and secondary structure. Within the substructure of the angular profiles are the first unambiguous experimental observations of sideband diffraction. A comparison of the experimental results and the theoretical predictions of different models is made.

I. INTRODUCTION

In this paper we present a study of elastic and inelastic scattering of low-energy electrons from a clean (100) surface of aluminum in the energy range $0 \lesssim E \lesssim 300$ eV. In this energy range, the electron interactions with the metallic-ion cores and valence electrons are so strong that they penetrate only a few atomic layers into the bulk. An analysis of their inelastic differential cross sections permits the determination of the dispersion relations for various electronic excitations in the metals and the nature of the coupling between the probe electron and the excitation.[1-3]

In Paper I[4] we presented preliminary results of electrons which had undergone inelastic low-energy-electron diffraction, together with the initial interpretations. Since that time, more results have been obtained and the interpretations expanded and partially revised. It is the purpose of this paper to present these new results and interpretations, together with the details of the experimental procedure.

Measurements of the absolute intensities are reported for both the elastic and inelastic electrons diffracted into nonspecular directions. These measurements are then compared with the predictions of various models which describe elastic[5-11] and inelastic[1-3,12-14] low-energy-electron diffraction. The objective is not to measure the plasmon-dispersion relations from these results, but to check the consistency of the results with the models' predictions. It has been shown[8] that the large-angle elastic scattering, such as seen in the nonspecular diffraction, is more difficult to analyze than the smaller-angle specular scattering. The uncertainty in the elastic scattering carries over to the analysis of the inelastic scattering and makes quantitative analysis difficult. However, it is still possible to extract from the data useful qualitative results, especially since the surface-plasmon and bulk-plasmon losses are easily identified in aluminum.

It will be demonstrated that the experimental measurements are consistent with the two step model of inelastic low-energy-electron diffraction (ILEED). In particular, a single-step model of the loss process is inadequate in describing the results. The phenomenon of sideband diffraction[12,13] is observed in the angular profiles of electrons which have excited bulk plasmons. Structure is seen in the inelastic-energy-intensity profile of these electrons which might also be due to sideband diffraction, although recent calculations[3] indicate that similar structure can be accounted for by multiple elastic scattering.

In Sec. II the historical and theoretical foundation for this work is briefly reviewed. Section III is devoted to a description of the apparatus and the experimental procedure. It includes a discussion of the preparation and cleaning of the target surface, as well as a discussion of how the surface conditions are monitored.

Section IV contains measurements of

$$\frac{d^2\sigma(E_p, w, \theta_s, \phi_s)}{d\Omega_s\, dE_s} ,$$

i.e., the elastic ($w = 0$) and inelastic ($w \geq 0$) differential scattering cross section for electrons incident in a normal direction on the target crystal. In this expression, E_p is the energy of the incident electron, $E_p - w$ is the energy of the scattered electron, and θ_s, ϕ_s are the scattered polar and azimuthal angles, respectively. Absolute-intensity

measurements of the differential cross sections as a function of these parameters are presented.

The experimental measurements are displayed in three forms: energy-intensity profiles, energy-loss profiles, and angular profiles. The energy-intensity profiles are plots of the scattered intensity as a function of the incident or primary energy E_p. The energy-loss profiles are plots of the scattered intensity as a function of the energy loss w, and the angular profiles are graphs of the intensity as a function of the scattered polar angle or collector angle θ. In measuring the energy-intensity profile of a nonspecular diffraction beam, we vary θ to follow the beam as it moves in space as a function of E_p. Except for this, the other parameters were held constant for each profile measurement. We selected ϕ_s to obtain the desired $\bar{g}=(h, k)$ diffraction direction. A general discussion of the results is given in this section together with the experimental measurements.

Section V is a comparison of the experimental results with some theoretical predictions of both the elastic and inelastic profiles. It is found that the absolute intensities, both elastic[8] and inelastic,[2,15] are predicted by an expanded version of the inelastic-collision model. The two-step-diffraction version of this model also predicts the main features of the inelastic cross sections. Finally, in Sec. VI, a summary of the results and the conclusions drawn from them is presented.

II. THEORETICAL PRELIMINARIES

In 1927, Davisson and Germer[16] discovered that electrons can diffract coherently from a single-crystal lattice. The phrase low-energy-electron diffraction (LEE) has been applied to this phenomenon involving electrons with energies in the range $15 \lesssim E \lesssim 300$ eV which have elastically scattered from the lattice. Electrons which undergo elastic and inelastic low-energy-electron diffraction are denoted by ELEED and ILEED, respectively. Included in ELEED are those electrons that have lost an amount of energy that is nonresolvable with my instrument, such as by phonon stimulation. There are currently several good reviews[17–20] that trace the historical development and uses of ELEED, so that topic will not be pursued here. A typical energy distribution for a monoenergetic beam of electrons scattered from a metal is usually divided into three regions—elastics, inelastics, and true secondaries. The elastics are electrons that, within the experimental energy resolution of the analyzer, have scattered from the crystal with no energy loss. The inelastics are electrons which have scattered from the crystal and in the process have lost a characteristic amount of energy. Any structure which is classified as inelastic is found with a nearly constant energy difference w from the elastic electrons at E_p, regardless of the value of E_p. The phrase "nearly constant" is used because any given loss mechanism may produce structure within a small region of w, the exact value of w depending on dynamical scattering effects. The true secondaries and Auger electrons are found at nearly constant secondary energies, regardless of the value of E_p. They were not studied as a part of this work.

In constructing a model of ILEED, it is necessary to know the loss mechanism that produced a certain structure in the inelastic-energy region. Aluminum is one of the few materials in which the loss mechanism creating the primary structure in the inelastic-loss profile is generally accepted to be excitation of bulk and surface plasmons. High-energy-electron-transmission experiments,[21,22] high-energy back-scattering experiments,[23] and optical-reflectivity experiments[24] have been compared with theoretical predictions[25,26] with the conclusion that in Al, the infinite-wavelength bulk plasmon occurs near 15 eV and the surface plasmon near 10 eV.

Since the discovery of LEED, a number of experimental studies[16,27–34] have demonstrated the connection between ELEED and ILEED involving low-energy losses ($1 \lesssim w \lesssim 30$ eV). These studies led to the identification of a two-step process of inelastic diffraction as the primary mechanism in which inelastically scattered electrons escape the crystal. In this process, the detected electron can undergo elastic scattering from the crystal lattice (diffraction) and inelastic scattering (creation of a plasmon, etc.) in either sequence. There have been several formal analyses[35–37] of ILEED using a quantum field theory. However, Duke and Laramore,[12,13] having expanded upon the elastic theory of Duke and Tucker[5] and Duke, Anderson, and Tucker,[6] have developed the only detailed theoretical calculations of ILEED intensities using a quantum-field-theory approach. A basic ingredient in this theory is the systematic utilization of a set of "surface" conservation laws of energy and momentum parallel to the surface. Their initial calculations first were extended to provide detailed predictions of inelastic scattering from clean Al surfaces. Subsequently, Duke and Landman[3] extended the two-step analysis of Duke and Laramore[12,13] and of Duke and Bagchi[1–3] to include the effects of multiple elastic scattering. They concluded that these effects are important primarily in the energy profiles of the inelastically scattered electrons. Hence, the detailed analysis of my data is confined to the loss and angular profiles.

Because of the magnitude of the works just referenced, only a summary here of the types of effects expected will be presented. A process in

which the electron undergoes an elastic diffraction from the lattice followed by an inelastic collision, such as in plasmon creation, is called an elastic-inelastic (EI) process. The reverse process of an inelastic diffraction will be called an IE process. In either process, the conservation laws of energy and momentum parallel to the surface are obeyed for each interaction (E or I), and consequently between the incident and final electron states. If the electron scatters coherently from successive layers of the lattice, a resonance occurs which, in lowest-order perturbation theory, is the familiar Bragg scattering. This manifests itself in the elastic-energy-intensity profile as a peak at an energy called a Bragg energy E_{Bragg}.

A peak in the energy intensity profile is expected for loss energy w whenever the energy of the beam undergoing elastic diffraction equals E_{Bragg}, guaranteeing the conservation of total momentum at the elastic vertex. This condition will be met once for the EI process at $E_p \approx E_{\mathrm{Bragg}}$ and once for the IE process at $E_p \approx E_{\mathrm{Bragg}} + w$. These equations hold if the excitation momentum and energy are small compared to the incident-electron momentum and energy, as is the case with the surface and bulk plasmons considered here. Besides these maxima, Duke and Laramore[12,13] predicted a maximum in the scattered intensity to occur whenever the total crystal momentum is conserved, that is, when the sum of the incident-electron momentum, final-electron momentum, and excitation momentum equals a bulk reciprocal-lattice vector. They refer to such maxima as sideband-diffraction peaks. Their presence is expected to be observed in the angular profiles, possibly in the energy profiles, and probably in the energy-loss profiles of electrons which have excited bulk plasmons [or any bulk loss with wave vector $\vec{p}(w) \neq 0$]. The detection of the phenomena is dependent on the electronic properties such as the loss dispersion relation and electron damping and on the experimental energy and the angular resolutions. Unfortunately, however, it cannot be distinguished clearly in the energy profiles from multiple-elastic-scattering effects.[3]

Because of the localization of the surface-plasmon wave vector along the surface, the angular profiles of electrons which have excited surface plasmons are expected to consist of a doublet structure. The experimental measurement of this doublet structure depends upon the relative probabilities of each excitation direction, upon the dispersion relation, electron damping, and the energy and angular resolutions. The angular profiles of the electrons which have excited bulk plasmons usually are expected to consist of only a single peak. However, in regions of sideband diffraction, Duke and Laramore predicted that this singlet would become a doublet, changing back to a singlet again as the incident-electron energy was varied. For realistic values of the plasmon energy and momentum, this doublet is expected to occur for incident energies near $E_{\mathrm{Bragg}} + w$.

III. APPARATUS AND EXPERIMENTAL PROCEDURE

The basic instrument, shown schematically in Fig. 1 and consisting of a four-grid-retarding-field energy analyzer with a collimated Faraday collector, electron gun, target assembly, and electrostatic shielding, has been described previously.[4] The instrument is enclosed in a field-free region and is housed in an ultra-high-vacuum chamber whose base pressure during experimental measurements is about 1×10^{-10} Torr.

The target is an ultra-high-purity (99.999%) Al single crystal,[38] $3.8\times0.9\times0.24$ cm in size with a 0.08-in. hole drilled near the top to permit attachment to the Al holder. This hole was spark cut so that little or no mechanical damage was introduced into the experimental region. The crystal is held in place by clamping it against a slot in an Al block. This slot prevents the crystal from rotating in the holder about an axis perpendicular to the face of the holder. The block, clamp, and screw are made of ultra-high-purity aluminum to prevent impurities from migrating to the target during annealing. This assembled block is bolted to the remaining target assembly and is aligned so that the incident electron beam impinges normally on the crystal surface. The aluminum crystal was prepared using the methods previously described.[4] After mechanical and chemical polishing, the crystal was electropolished (to remove fine scratches, etc.) for a few minutes in a solution[39] of ethanol and perchloric acid. The perchloric acid polishing solution was chosen over others primarily because it is thought to leave[40] a relatively thin (~30 Å) oxide layer on the surface.

The crystal surface was cleaned in vacuum using

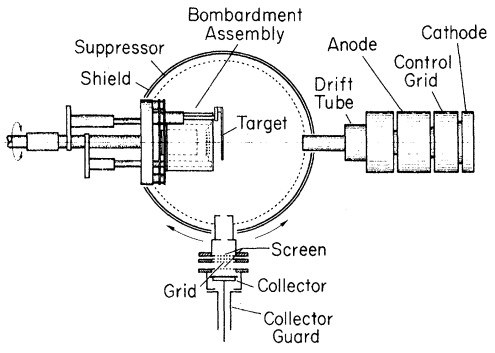

FIG. 1. Schematic of the energy–angular-distribution instrument showing the basic components.

the Farnsworth method of argon-ion bombardment introduced for Al by Jona[41,42] and verified by others.[40,43,44] Five or six treatments consisting of bombardment followed by annealing produced a clean surface.

Four basic tests of the cleanliness of our target surface were used. The least sensitive, but one which gives the order of magnitude of cleanliness and is most attainable, was the reproducibility of the ELEED pattern and the energy profile. The observed Auger spectra of the surface after multiple cleanings showed no evidence of contaminants. However, the present apparatus was not designed to do high-sensitivity Auger work (better than ~0.1 monolayer sensitivity).

It is possible to monitor the surface cleanliness to coverages less than the ~0.1 monolayer of O_2 coverage provided by the Auger measurements by using the technique of electron-loss spectroscopy and the reproducibility of the surface-plasmon-loss profiles. It has been found both by the author and by Edwards[45] that when O_2 is added to a clean surface of W, a new peak in the energy-loss profiles may be measured near 7 eV. This author determined that it is most easily found near energy and angular conditions of Bragg resonances, and its presence is detectable with about 0.05 monolayers of O_2 on the surface, using accepted values of the sticking probabilities. This loss peak was also measured on the Al surface in the presence of O_2. If the same sensitivity as on W is assumed, then the Al surface is free of O_2 to less than 0.05 monolayers. The surface-plasmon-loss peak near 10 eV was also present during the measurements on Al.

The most sensitive test to change appears to be the reproducibility of the surface-plasmon-angular and -loss profiles. Changes in the peak positions and intensities could be measured about 8 h after argon bombardment and annealing, or with about 0.02 and 0.03 monolayer coverage of background (mostly H_2) gas, or $\lesssim 0.01$ monolayer of O_2 (using the values of the sticking coefficients as determined by Jona[41] and Marsh[40]).

All measurements reported here as being taken on a clean surface of Al were taken within 5–6 h after each sputter-anneal cycle and in a background pressure of $\sim(1-2)\times10^{-10}$ Torr. Thus, no more than 0.01–0.05 monolayer of adsorbate on the surface is expected during our clean measurements.

IV. EXPERIMENTAL RESULTS AND DISCUSSION

This section contains the presentation of the experimental measurements and a general discussion of the results, whereas Sec. V presents a detailed comparison of the theoretical profiles and experimental measurements. The profiles will be presented in a set of normalized units, so that the diffracted-beam intensities can be compared with each other and with the intensity of the incident beam. The method for making these comparisons, the first of their kind for inelastically diffracted electrons, together with an intensity analysis is given in Sec. IV A. The subsequent Secs. IV B–IV D contain the presentation of the energy, loss, and angular profiles, respectively. The work-function difference between the aluminum target and the tungsten-wire retarding grids and tungsten cathode, ~0.25 eV, has been accounted for in the energy measurements.

A. Measurement of the Absolute Intensity

The object of these measurements was to determine the percentage of electrons scattered into a particular region of the energy-angle space (an absolute-intensity measurement), and then use this as a calibration for the rest of the measurements. To accomplish this, one must: (i) measure the total electron current incident on the target, (ii) measure the electron current scattered into a particular beam in the desired energy-angle space, and (iii) compare the experimental measurement (detector output) of this beam profile with the scattered percentage of incident current to get a conversion factor for the electronic output.

Figure 2 shows the measurements made in a calibration experiment to determine the desired conversion factor. In this calibration run, the incident-electron current to the target I_0 was 5.0×10^{-6} A, which is the sum of the target current and the current to the electronic shielding. Since the electron gun is the only source of electrons and since the current is conserved, this measurement gives the total incident current. Next, an angular profile of the elastically scattered electrons was taken, as shown in Fig. 2(b). To measure the currents, the collector was located at 34°, to correspond to the peak in the elastic-angular profile. Then, the retarding-energy curve and the energy-loss profile were measured, as shown in the other two panels. For a collector of energy-acceptance width approximately equal to the incident-electron-beam width, about 1 eV in this case, the total scattered elastic current is approximately the current at a loss energy equal to the energy width. In these measurements it was found that I(elastic) $= 0.1\times10^{-8}$ A.

The measured height of dI/dE for the elastic beam is 0.76 units; these units are applicable when the values of all variables such as amplifier gain, etc., as determined in the calibration experiment are used. Then an experimental height of 0.76 units corresponds to a percentage reflection equal to $\frac{1}{5}(0.1\times10^{-8})/10^{-6}$ or 0.02% I_0. Thus, one unit equals approximately 0.026% I_0. This factor has been applied to all the measurements, with proper

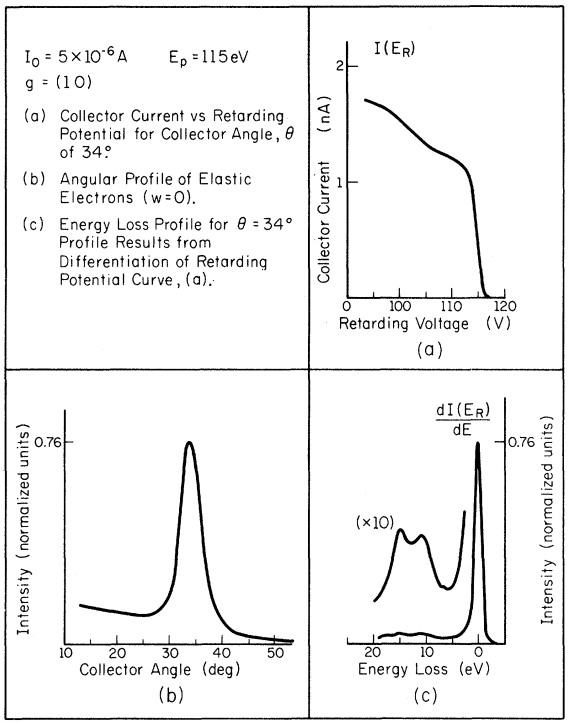

FIG. 2. Experimental measurements necessary to calibrate the intensity of the scattered electrons.

account being taken for amplifier gain, etc. To make the measurements easier, the scale is converted to "normalized units," in which one normalized unit equals 0.01% I_0. If a curve has been amplified for clarity, this will be denoted on the profile as a gain in parenthesis after the fixed variable, such as E_p = 100 eV (×10), indicating that the particular profile is for a primary energy of 100 eV and is shown amplified by a factor of 10. For convenience, the amplification factor has been included on the intensity scale shown on the experimental profiles. Thus, the absolute intensity of each curve can be read directly from the graphs.

B. Energy-Intensity Profiles

The elastic and inelastic energy-intensity profiles discussed are those of the (11) diffraction beam resulting from the diffraction of electrons incident normally on a clean (100) surface of Al. In obtaining the energy-intensity profiles, a series of angular profiles was taken over the range of incident-electron energies for each desired loss energy. The intensity was then measured at the desired collector angle by subtracting the extrapolated incoherent background in the angular profile and normalizing to unit incident beam current. The inelastic intensity for each incident energy was measured at the collector angle at which the elastic-angular profile at that incident energy was maximum, called θ_{elastic}. Figure 3 shows the measured elastic ($w = 0$) and inelastic (w = 8–18 eV) energy-intensity profiles for the (11) diffraction beam. Similar profiles of the (10) beam were shown in Paper I.[4] The elastic profile of the (10) beam is also shown in Fig. 6 of this paper.

1. Elastic Energy-Intensity Profiles

The (11) profile has three major peaks at 43, 86, and 152 eV. The major peaks are distinct, well separated in energy, and of halfwidth 10–12 eV. These peaks correspond to kinematical Bragg peaks resulting from a single scattering if an inner potential correction of about 14 eV is used. This is most easily seen by comparing the experimental-peak locations with those predicted theoretically by Laramore and Duke[8] and found in Table I. The inner potential of 14 eV locates all of the experimental peaks within 1 eV except for one which is within 2 eV.

The elastic measurements can also be compared with those of Jona[42] and Farrell and Somorjai.[46]

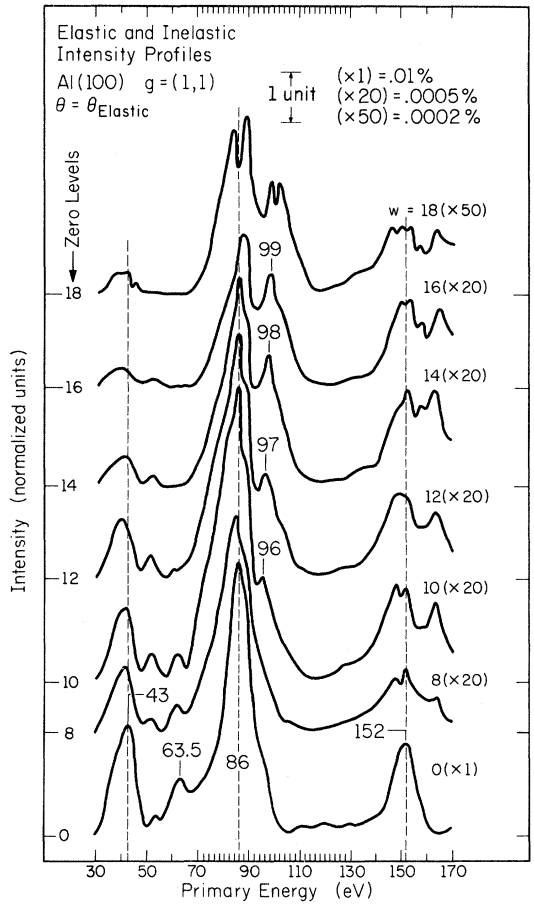

FIG. 3. Elastic and inelastic energy-intensity profiles for the (11) diffraction beam with normally incident electrons.

TABLE I. Comparison between experimentally observed and theoretically predicated positions of the principal peaks (in eV) in the elastic intensity profiles of the (11) and (10) diffraction beams from Al(100). V_I is the inner potential correction (in eV).

Experimental			Theoretical	
Jona[a]	Farrell and Somorjai[b]	This work	Laramore & Duke[c] V_I=14	Marcus *et al.*[d] V_I=7.5
		(11) beam		
46		43	43	46
90	88	86	87	90
151	143	152	151	
		(10) beam		
56	55	54	53	56
84	74	(75)	75	79
105	98	107	105	105

[a]Reference 42.
[b]Reference 46.
[c]Reference 8.
[d]Reference 47.

Their experimentally determined peak locations are also found in Table I. For the most part, the agreement with the work of Jona is good, while that with Farrell and Somorjai is adequate.

There are two low-energy peaks in the (10) beam profile at 33 and 40 eV. The (11) profile shows two peaks at 54 and 63.5 eV and some less prominent peaks at 112, 121, and 130 eV. Jona's profiles show these secondary peaks near 34 and 42 eV in the (10) profile and at 69 and 120 eV in the (11) profile. These are probably multiple scattering resonances, as we see in Sec. V.

2. *Inelastic Energy-Intensity Profiles*

An examination of the inelastic-intensity profiles shows that the structure for each loss energy is closely correlated with the structure in the corresponding elastic profile. For example, the gross structure in the inelastic profile occurs at about the same energies as the structure in the elastic profile.

Confining our attention to the energy region around the major peaks in the elastic profile, we first note that a peak occurs in the inelastic profiles at about the energy that the elastic profile has a Bragg peak (within 1 eV). This inelastic peak at E_{Bragg} is principally associated with those electrons whose scattering amplitude for elastic diffraction followed by an inelastic scattering (EI) is large.

We also expect to see a peak in the inelastic profile for loss energy w at $E_{\mathrm{Bragg}}+w$, which is principally associated with those electrons whose scattering amplitude for an inelastic scattering followed by elastic diffraction is large (IE scattering). Indeed, peaks are experimentally observed at $E_{\mathrm{Bragg}}+w$ within $\pm$ 1–2 eV for a majority of the inelastic energy profiles in both the (10) and (11) diffraction beams. The clearest example of this is seen around the (11) Bragg peak at 86 eV. For electron losses between 10 and 16 eV, we find a prominent peak at 86 eV, corresponding to EI scattering, and a second peak located above this which moves away in energy as the loss energy increases, corresponding to IE scattering.

However, for a loss energy of 18 eV, the inelastic profile around E_p = 86 eV has become a four-peaked structure. As the electrons which have lost 18 eV are those which have primarily excited bulk plasmons, the presence of four peaks is an indication of possible sideband diffraction. Recent calculations by Duke and Landman[3] indicate that the four-peaked structure in the inelastic energy profiles can also be an effect of multiple scattering. The phenomenon of sideband diffraction is evident, however, in the inelastic angular profiles.

Included in this figure are the first absolute intensity measurements for differential cross sections of inelastically back-diffracted electrons, expressed as a percentage of the incident-beam current. At the Bragg energies, the surface-plasmon losses are about 5% of the elastic intensities, and the bulk plasmons are about 2% of the elastic intensities. These numbers are in good agreement with the theoretical expectations.[2,13]

C. Energy-Loss Profiles

Figure 4 shows a series of energy-loss profiles. As discussed in Sec. II, the prominent peak near w = 10 eV corresponds to the excitation of a surface plasmon, the peak near 15 eV to the excitation of a bulk plasmon. While not shown in this figure but shown in Paper I, we observed the presence of other loss peaks at 26 and 31 eV, a series of loss peaks between 4.0 and 6.0 eV, and one at 8.0 eV. We now suspect that the 4–6 eV losses are due to a single loss mechanism, such as an interband transition, and the 8 eV loss is due to a separate, but unknown loss mechanism.

Figure 4 shows a series of energy-loss profiles taken at different primary energies (E_p = 80–100 eV) and at three different relative collector angles. $\theta_{\mathrm{elastic}}$ is defined as the angle at which the elastic angular profile is a maximum. In other words, it is the angle relative to the surface normal at which the wave vector of the diffracted electron intersects the reciprocal-lattice rod in an Ewald construction. The various primary energies have been chosen so as to encompass the (11) Bragg energy at 86 eV. Recalling Fig. 3, it is seen that this choice of primary energies moves from a range primarily of EI diffraction to a range primarily of IE diffraction. This, then, demonstrates

the effects of different diffraction conditions on the energy-loss profiles.

The most obvious feature evident in the figure is the relative growth and decay of the surface and bulk plasmons as a function of primary energy and scattering angle. First, for the collector angles constant with respect to θ_{elastic}, we note that for primary energies below the Bragg energy, there is a large surface-plasmon-loss peak at $w = 10$ eV and only a shoulder of a bulk-plasmon-loss peak. As the incident energy increases through the Bragg energy, the bulk-plasmon loss grows relative to the surface plasmon until, at $E_p = 100$ eV, there is a large bulk-plasmon-loss peak at $w = 15$ eV and only a shoulder of a surface-plasmon loss. The rate of increase and decrease is dependent on the angle relative to θ_{elastic}, as can easily be seen by comparing the three panels. This also is evident upon comparing the profiles for a constant incident energy, for example, those of $E_p = 95$ eV. For a collector angle less than θ_{elastic}, the loss profile consists of a large surface-plasmon loss and a shoulder of a bulk-plasmon loss. As the angle is moved to angles greater than θ_{elastic}, the profile consists of a large bulk-plasmon loss and a shoulder of a surface-plasmon loss.

Examination of the loss profiles also shows that the positions of the peaks are a function of the primary energy. For instance, at θ_{elastic}, the surface-plasmon-loss peak is at 10 eV for $E_p = 80$ eV and at about 11 eV for $E_p = 95$ eV. One can ask whether this shift is a real change as a function of different diffraction conditions, or whether it is an apparent change caused by the addition of a large bulk-plasmon peak located near the surface plasmon. If we assume that the loss peaks are Gaussian curves with widths equal to the experimental widths (~ 2 eV) and separated by 5 eV then a numerical calculation shows that the addition of a second peak which is equal in height to the first will shift the first peak position by about 0.3 eV. Thus, the 1-eV experimental shift probably is a real shift which is a function of the incident-electron energy. That this shift is real is further substantiated by comparison with the theoretical profiles in Sec. V in which it is seen to be a direct result of diffraction phenomena described by the two-step model of ILEED.

D. Angular Profiles

Figure 5 shows a series of angular profiles at a constant primary energy ($E_p = 92$ eV). Note that the elastic profile ($w = 0$) is symmetrical and well localized in angle in what is commonly called a diffraction beam. If the inelastic profiles ($w \neq 0$) are examined, it is seen that they too are found in localized beams which occur near the elastic beam. This is a consequence of inelastic two-step diffraction. Without a diffraction from the lattice, we would not expect to find the inelastics so well localized in angle. But there are dynamical scatter-

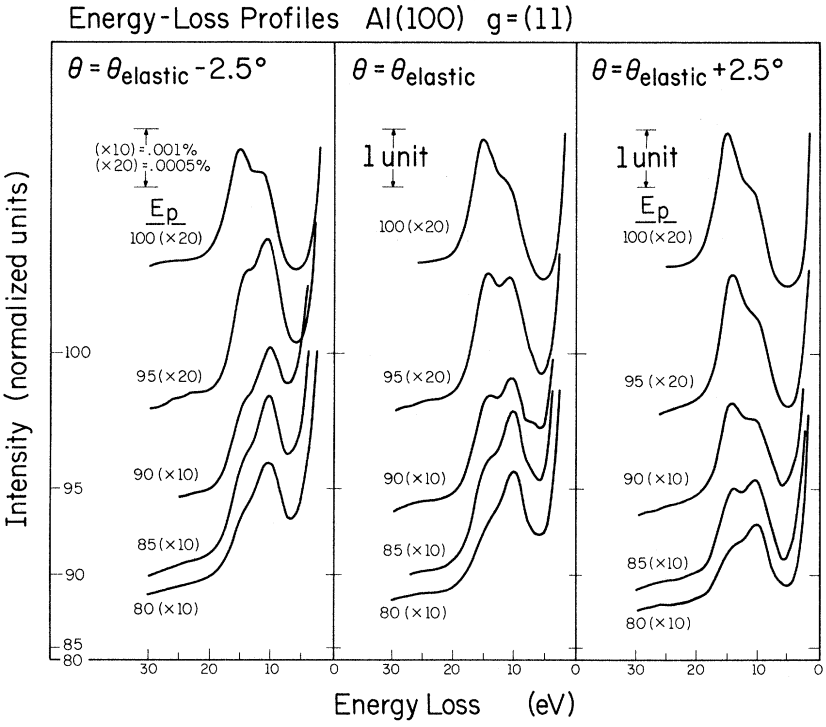

FIG. 4. Series of energy-loss profiles in the (11) diffraction beam for different primary energies E_p and collector angles θ. The ordinate marks correspond to the zero levels of each profile.

ing effects present, as can be seen in the internal structure of the inelastic profiles.

The angular profiles for the $w = 12$ and 13 eV losses have the doublet structure that is expected for electrons which have excited surface plasmons. This doublet structure was seen in some of the loss profiles which were shown in Paper I. The angular profiles of the electrons which have lost more energy, $w = 14-18$ eV, have either a more complicated structure or consist of a doublet. The theoretical calculations[13] have predicted that a doublet structure in the bulk-plasmon angular profiles is possible evidence of sideband diffraction.

However, certain structure can be associated with a surface-plasmon loss and hence the cause of an apparent splitting. For instance, as shown in Fig. 5, the surface-plasmon peak beginning at

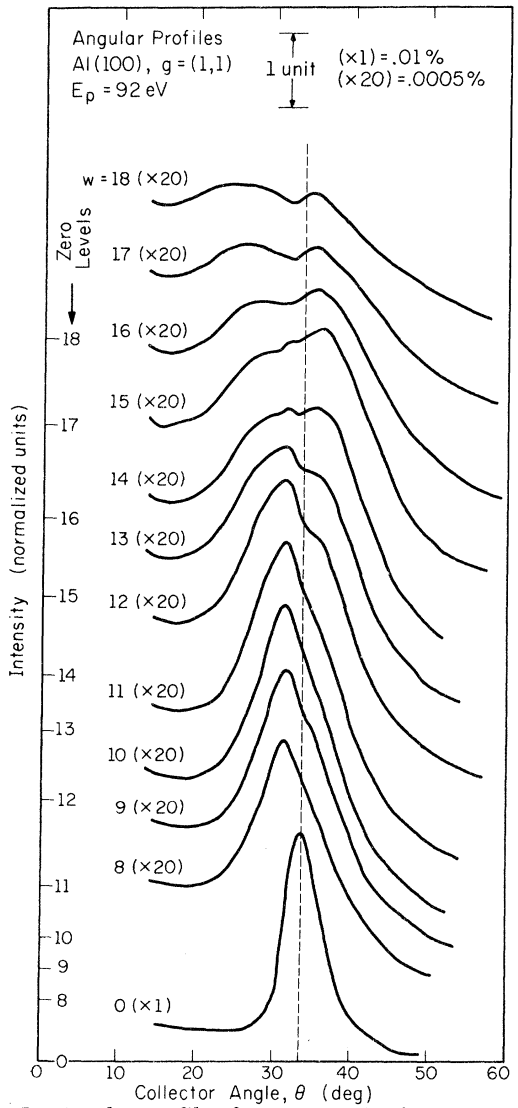

FIG. 5. Angular profiles for a constant primary energy (92 eV) and different loss energies.

10 eV is observed to move to slightly lower angles as the loss energy is increased to 13 eV. As the loss energy is increased to 17 eV the surface-plasmon peak moves out more rapidly to lower angles, a consequence of the increasing plasmon wave vector. But at the same time another peak is seen just to the low-angle side of the elastic peak to grow for $w = 14$ and $= 15$ eV. This peak, together with the peak on the high-angle side is a bulk-plasmon peak. The surface-plasmon peak on the high-angle side of the elastic peak for $w = 12$ and 13 eV has decreased in intensity and moved to higher angles by the time $w = 14$ and 15 eV. Thus, the two peaks located on either side of the elastic peak (by $1°-1.5°$) in the $w = 15$ eV profile comprise a bulk-plasmon doublet due to sideband diffraction. The third peak in the $w = 15$ eV profile is located 7° to the low-angle side of the elastic peak. Using the law of conservation of momentum parallel to the surface, a straightforward calculation leads to the result that the excitation's momentum parallel to the surface for this peak is about 0.6 Å^{-1}. As shown in Sec. V and Refs. 1–3, this value is far too big for a bulk plasmon near this energy loss, but is about correct for a surface plasmon. Another analysis, although qualitative, leads to the same conclusion. If Fig. 8 is reexamined, it is seen that for $E_p = 90$ eV and $\theta < \theta_{\text{elastic}}$, the energy-loss profile indicates that the 15-eV loss has a stronger surface-plasmon component than bulk plasmon. However, for $\theta \gtrsim \theta_{\text{elastic}}$, the bulk-plasmon component dominates at $w = 15$ eV is what was just concluded from the angular profiles. The phenomenon of sideband diffraction is also present in the $w = 16$ eV profiles of Paper I, although one must carefully examine curves similar to Fig. 5 (shown here) to be sure of the correct identification.

In addition to identifying the dynamical origin of various details in the measured intensities, the dispersion relations of the surface and bulk plasmons can be determined from plots such as shown in Fig. 5. This can be done by either making a straightforward kinematic calculation, using the law of conservation of momentum parallel to the surface, as done in a preceding paragraph, or by using a quantum-field-theoretical (QFT) treatment as done by Duke and Bagchi.[1,2] The QFT treatment should yield a more accurate dispersion relation, because it takes account of the various dynamical scattering factors present. We refer the interested reader to Refs. 1 and 2 for details of the calculation.

V. COMPARISON OF EXPERIMENTAL AND THEORETICAL PROFILES

In this section, some of our experimental profiles are compared with some theoretical profiles

calculated by Duke and Bagchi,[1,2] Laramore and Duke,[8] Hoffstein and Boudreaux,[9] Jepsen, Marcus, and Jona,[10] Hirabayashi,[11] and Marcus, Jepsen, and Jona.[47] The profiles calculated by Duke and Bagchi are those describing the inelastic scattering intensities. The profiles calculated by the other authors are those describing the absolute elastic scattering intensities.

There are substantial differences in the models used in these sets of theoretical calculations. Laramore and Duke used a finite-temperature version of the inelastic-collision model[5,6] with an electron–ion-core potential described by s-, p-, and d-partial-wave phase shifts to describe the elastic scattering from the solid. Bagchi and Duke, on the other hand, used an isotropic scattering version (s-wave scattering only) of the inelastic-collision model which was also temperature independent in order to calculate a series of inelastic profiles. The less-complete latter model was used only for those calculations of the angular and loss profiles for which they have been shown to be adequate.[4]

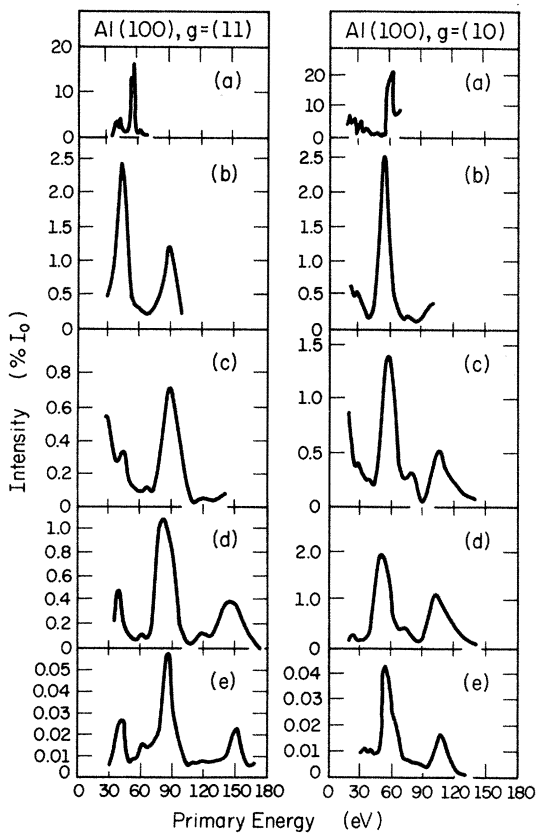

FIG. 6. Theoretical (a)-(d) and experimental (e) elastic energy-intensity profiles in the (11) and (10) diffraction directions. The theoretical profiles are by (a) Jepsen *et al.* (Ref. 10), (b) Hirabayashi (Ref. 11), (c) Marcus *et al.* (Ref. 47), and (d) Laramore and Duke (Ref. 8). Our (11) and (10) beams, labeled using a primitive unit cell, are equivalent to the (20) and (11) beams, respectively, of Refs. 10, 42, and 47.

Jepsen, Marcus, and Jona's calculations were carried out using a method referred to as the layer-Korringa-Kohn-Rostoker (KKR) method,[48] which combines a treatment of multiple scattering in each layer by the KKR method of band theory with a propagation-matrix method of handling multiple scattering between layers in a beam representation. Their calculations for the absolute reflected intensities did not consider inelastic damping, as they used a real potential in the scattering. However, they calculated other elastic intensity profiles using an imaginary part of the potential to account for inelastic scattering when they fit the position and shapes of the experimental curves. Marcus *et al.* also used the layer-KKR method for their calculations. They included a real and imaginary part of the scattering potential to account for damping and they also allowed for temperature dependence in their calculations.

Hoffstein and Boudreaux used a band-structure-matching approach with no inelastic damping and with a pseudopotential based on the orthogonalized-plane-wave (OPW) approximation without any adjustable parameters. Finally, Hirabayashi used a "simplified" version of the s-wave inelastic-collision model with no temperature dependence.

The results of four of the authors are shown in Fig. 6, together with our measured experimental profiles. The results of Hoffstein and Boudreaux were qualitatively similar to those of Jepsen *et al.* but more difficult to reproduce in the figure shown. Unfortunately, even the results of Jepsen *et al.* lose some detail when reproduced on such a reduced scale. They are shown for rough comparison only; the fine structure can easily be seen in the original work. As is readily seen, the best agreement between experiment and theory is found with the profiles calculated by Laramore and Duke and Marcus *et al.* The two will now be compared in more detail.

The theoretical and measured line shapes of both the (10) and (11) beams agree well. The major peaks are in about the same places (refer to Table I), the relative sizes of the peaks are about right, and the secondary structure also is reproduced. See, e.g., the multiple scattering peak at about 62 eV in the (11) profile. The profiles differ in that the experimental peaks are about half as wide as the theoretical peaks.

The absolute intensities of the calculated and observed peaks are found to be in qualitative agreement and in the best quantitative agreement obtained so far. The absolute intensity of the (11) Bragg peak at 86 eV was measured to be 0.056% I_0, where I_0 is the intensity of the incident electron

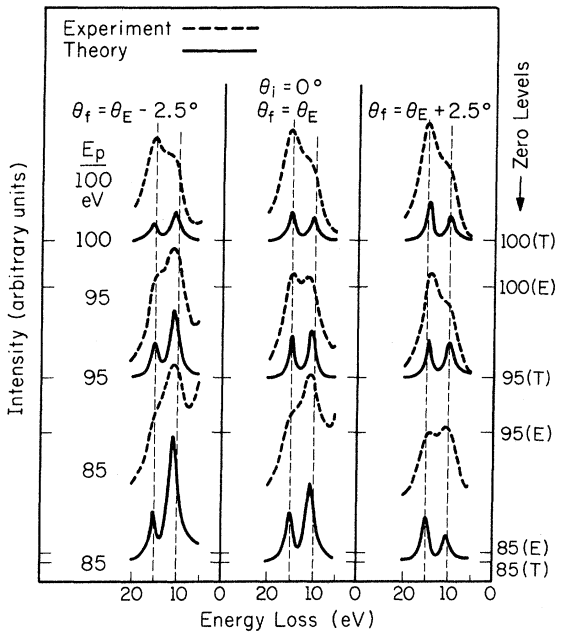

FIG. 7. Theoretical and experimental energy-loss profiles in the (11) diffraction direction. The theoretical profiles were calculated by Duke and Bagchi (Refs. 1 and 3). The ordinate marks are the zero levels for theory (T) and experiment (E).

beam. The absolute intensity of the (11) Bragg peak at 86 eV was calculated to be about 0.7% I_0 by Marcus *et al.* and about 1.1% by Laramore and Duke, or 12.5 and 19.5 times larger than experiment. The agreement of the theory with the other experimental (11) peaks is equally good. The calculated intensities of the (10) Bragg beams are about 35 to 50 times larger than the experimental measurements. In general, the agreement between the calculated and observed intensities is surprisingly good with regard to the absolute magnitude, as well as the line shape of both the elastic and inelastic intensities. Although the models used by Laramore and Duke and by Marcus *et al.* in the calculations are simplified, they seem to describe the scattering phenomena quite adequately.

Finally, a set of inelastic profiles calculated by Duke and Bagchi are examined. It was found[2] that the empirical electron-plasmon vertex used by Duke and Bagchi in the two-step model does, in fact, give approximately the correct relative intensities of the elastic and inelastic cross sections. Thus, the theoretical and experimental inelastic profiles can be compared on approximately the same scale as the elastic profiles. Figure 7 shows a series of experimental and theoretical energy-loss profiles, equivalent to the conditions described for Fig. 4. As the primary energy increases above the Bragg energy at 86 eV, the strength of the bulk-plasmon loss peak grows relative to that of the surface plasmon. This is seen in both the experimental and theoretical curves. Differences in relative intensities of the two losses can be explained by remembering that the experimental profiles contain the electrons which have scattered both coherently and incoherently from the solid, as well as electrons which have excited particle-hole excitations.

Figure 8 shows a set of theoretical and experimental angular profiles for $w = 14$ eV. The theoretical profiles were calculated with a set of parameters for illustrative purposes only. The theoretical profiles show the two surface-plasmon peaks on the very-low- and very-high-angle sides of θ_{elastic} at $E_p = 84$ eV, after which it becomes a doublet about θ_{elastic} for $E_p = 88$ and 90 eV. For larger values of E_p, the peak gradually becomes a single peak located on the high-angle side of θ_{elastic}. This is the behavior seen in the experimental profiles. As was pointed out in Fig. 5, the low-angle surface plasmon and the two bulk-plasmon peaks due to sideband diffraction at $E_p = 90$ eV are clearly seen.

VI. SUMMARY OF RESULTS AND CONCLUSIONS

The data presented in Secs. IV and V demonstrated clearly the existence of inelastic low-energy-electron diffraction. At the same time, the two-step model of ILEED was verified, by virtue of our reporting two peaks in the inelastic energy-intensity profiles representing EI and IE diffraction, and measuring the predicted[1,2] systematic correlations between the elastic and inelastic angular profiles based upon this model.

Examining the inelastic profiles in detail, the

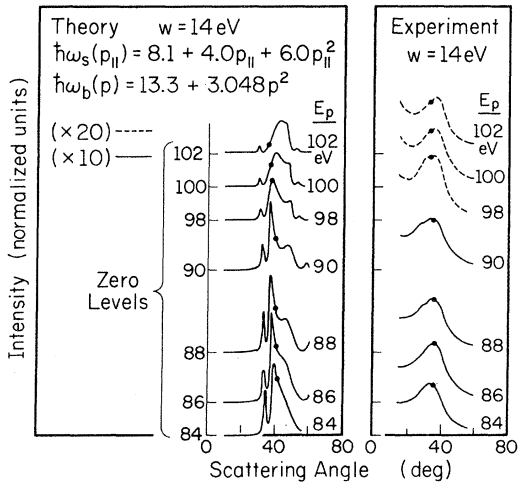

FIG. 8. Theoretical and experimental inelastic angular profiles in the (11) diffraction direction for a loss energy of 14 eV. The theoretical profiles were calculated by Duke and Bagchi (Refs. 1 and 3).

dependence of inelastic diffraction on different diffraction conditions was established. The energy-loss profiles demonstrated a new behavior in the change in the relative heights of the surface- and bulk-plasmon losses as the primary energy is swept across a Bragg energy. This provides a new test in distinguishing between the two types of losses in materials where the losses are not clearly known. The predicted doublet structure in the surface-plasmon angular profiles which is due to the localization of the excitation momentum along the surface was observed. The first unambiguous experimental observation of sideband diffraction was reported for a bulk-plasmon excitation in the inelastic angular profiles.

The comparison of the experimental and theoretical profiles indicates that the inelastic-collision model yields an adequate description of elastic and inelastic low-energy-electron diffraction and that the layer-KKR model adequately describes elastic LEED. The experimental profiles, when coupled with the former model of inelastic diffraction, yield[1-3] an adequate description of the plasmon dispersion relations, coupling relations, damping parameters, etc., thus increasing our knowledge of the chemical and electronic properties of solid surfaces.

ACKNOWLEDGMENTS

The author is indebted to Professor C. B. Duke, Dr. G. E. Laramore, Dr. A. Bagchi, and Dr. U. Landman for many invaluable discussions concerning the theory of inelastic diffraction and for copies of their results pertaining to his experiment prior to publication; to Professor F. M. Propst for his helpful experimental contributions during the course of this work; to Dr. T. L. Cooper for designing and constructing the original instrument; to Professor M. Metzger, for supplying the aluminum crystal and his technical experience in its preparation; and to the technical staff of the Coordinated Science Laboratory for their enthusiastic and imaginative technical assistance in their respective fields.

---

*Work supported in part by the Joint Services Electronics Program (U.S. Army, Navy, and U.S. Air Force) under Contract No. DAAB-07-67-C-0199, in part by the American Chemical Society, petroleum Research Fund under Contract No. PRF 3668-A3,5, and in part by the Air Force Office of Scientific Research, Office of Aerospace Research, USAF, under Grant No. AFOSR-71-2034.

†Present address: General Motors Research Laboratories, Department of Physics, Warren, Mich. 48090.

[1](a) C. B. Duke and A. Bagchi, J. Vac. Sci. Technol. **9**, 738 (1972); (b) A. Bagchi *et al.*, Phys. Rev. Lett. **25**, 998 (1971).

[2]A. Bagchi and C. B. Duke, Phys. Rev. B **5**, 2784 (1972); and private communication.

[3]C. B. Duke and U. Landman, Phys. Rev. B **6**, 2956 (1972).

[4]J. M. Burkstrand and F. M. Propst, J. Vac. Sci. Technol. **9**, 731 (1972).

[5]C. B. Duke and C. W. Tucker, Jr., Surf. Sci. **15**, 231 (1969).

[6]C. B. Duke, J. R. Anderson, and C. W. Tucker, Jr., Surf. Sci. **19**, 117 (1970).

[7]C. B. Duke *et al.*, Surf. Sci. **27**, 523 (1971).

[8]G. E. Laramore and C. B. Duke, Phys. Rev. B **5**, 267 (1972).

[9]V. Hoffstein and D. S. Boudreaux, Phys. Rev. Lett. **25**, 512 (1970).

[10]D. W. Jepsen, D. M. Marcus and F. Jona, IBM Research Report No. RC3525 (15956), 1971 (unpublished); Phys. Rev. B **5**, 3933 (1972).

[11]K. Hirabayashi, Surf. Sci. **28**, 621 (1971).

[12]C. B. Duke, G. E. Laramore, and V. Metze, Solid State Commun. **8**, 1189 (1970).

[13](a) C. B. Duke and G. E. Laramore, Phys. Rev. B **3**, 3183 (1971); (b) G. E. Laramore and C. B. Duke, Phys. Rev. B **3**, 3198 (1971).

[14]C. B. Duke, A. J. Howsmon, and G. E. Laramore, J. Vac. Sci. Technol. **8**, 10 (1971).

[15]Corrections in the absolute intensity scales of Ref. 2 have been made by U. Landman and C. B. Duke. Reference 2 was corrected by changing from scattering to reflection boundary conditions and by changing the strength of the bulk plasmons by a factor of 2. Reference 8 was corrected by G. E. Laramore by changing the normalization factor by a factor of about 5.

[16]C. Davisson and L. H. Germer, Phys. Rev. **30**, 705 (1927).

[17]J. W. May, Ind. Eng. Chem. **57**, 18 (1965).

[18]J. J. Lander, Progr. Solid State Chem. **2**, 26 (1965).

[19]P. J. Estrup and E. G. McRae, Surf. Sci. **25**, 1 (1971).

[20]E. J. Scheibner and L. N. Tharp, Surf. Sci. **8**, 247 (1967).

[21]Summarized by O. Klemperer and J. P. Shepherd, Adv. Phys. **12**, 355 (1963).

[22]J. Swan, A. Otto, and H. Gellenzer, Phys. Status Solidi **23**, 171 (1967).

[23](a) C. Powell and J. Swan, Phys. Rev. **115**, 869 (1959); (b) C. Powell and J. Swan, Phys. Rev. **118**, 640 (1960).

[24]M. Williams, E. Arakawa, and L. Emerson, Surf. Sci. **6**, 127 (1967).

[25]R. H. Ritchie, Phys. Rev. **106**, 874 (1957).

[26]E. Stern and R. Ferrell Phys. Rev. **120**, 130 (1960).

[27]P. P. Reichertz and H. E. Farnsworth, Phys. Rev. **75**, 1902 (1949).

[28]J. O. Porteus, in *The Structure and Chemistry of Solid Surfaces*, edited by G. A. Somorjai (Wiley, New York, 1969), p. 12-1.

[29]M. P. Seah, Surf. Sci. **17**, 132 (1969).

[30]T. L. Cooper, Ph.D thesis (University of Illinois, 1970) (unpublished).

[31]T. L. Cooper, J. M. Burkstrand, and F. M. Propst, in Program of the Thirtieth Annual Conference on Physical Electronics, 1970 (unpublished).

[32]J. C. Turnbull and H. E. Farnsworth, Phys. Rev. **54**, 507 (1938).

[33]W. H. Weber and M. B. Webb, Phys. Rev. **177**, 1103 (1969).

[34]M. P. Seah, Surf. Sci. **17**, 161 (1969).

[35]E. Bauer, Z. Phys. **224**, 19 (1969).

[36]J. I. Gersten, Phys. Rev. **188**, 774 (1969).

[37]Y. H. Ohtsuki, J. Phys. Soc. Jap. **29**, 398 (1970).

[38]The crystal was obtained from Professor M. Metzger, Dept. of Metalurgy and Mining, University of Illinois.

[39]O. P. Arora and M. Metzger, Trans. Met. Soc. AIME **236**, 1205 (1966).

[40]J. B. Marsh, General Electric Technical Information Series, No. 68-C-287, 1968 (unpublished).

[41]F. Jona, J. Phys. Chem. Solids **28**, 2155 (1967).
[42]F. Jona, IBM J. Res. Dev. **14**, 444 (1970).
[43]W. D. Robertson, International Conference on Solid Surfaces, 1971, Boston, Mass. (unpublished); and private communication.
[44]D. T. Quinto and W. D. Robertson, Surf. Sci. **27**, 645 (1971).
[45]D. E. Edwards, Ph.D. thesis (University of Illinois, 1970) (unpublished).
[46]H. H. Farrell and G. A. Somorjai, Phys. Rev. **182**, 751 (1969).
[47]P. M. Marcus, D. W. Jepsen, and F. Jona, Surf. Sci. **31**, 180 (1972).
[48]D. W. Jepsen and P. M. Marcus, *Computational Methods in Band Theory* (Plenum, New York, 1971), p. 416.

PHYSICAL REVIEW B VOLUME 7, NUMBER 8 15 APRIL 1973

Generalized Cluster Theory of the Coherent-Potential Approximations for Disordered Systems

E-Ni Foo and Shyamalendu M. Bose
Department of Physics, Drexel University, Philadelphia, Pennsylvania 19104

M. Ausloos
Institut für Theoretische Physik, Freie Universität Berlin, 1 Berlin 33, Germany

(Received 4 November 1971; revised manuscript received 11 October 1972)

The coherent-potential approximation (CPA) has been generalized to a cluster theory of CPA (α_0) where the effects due to all possible scatterings from clusters consisting of all atoms residing within the α_0th-shell radius are taken into account in a self-consistent manner. The present theory is more general than most of the existing theories of CPA. The pair theory of CPA as proposed by Cyrot-Lackmann and Ducastelle is discussed in detail in the light of our theory. The limitations of their theory are discussed and it is shown that this pair theory is a special case of our theory. By considering an infinitely large cluster our theory can be made entirely self-consistent. The accuracy of our theory however depends on the size of the cluster (or the magnitude of α_0) that we choose for practical computations. The inverse of the number of nearest neighbor, z^{-1}, is argued to be a good expansion parameter. By applying the ideas of elementary perturbation theory to our T-matrix equations we have developed a diagrammatic-expansion scheme for our theory, which enables us to estimate the errors resulting from the choice of a finite-size cluster. It is shown that our diagrammatic scheme when applied to the single-site T-matrix equations gives a result which is equivalent to Yonezawa's cumulant method, but our method is more straightforward, easier to understand and has a strong theoretical foothold. This diagrammatic method is then extended to the case of multiple scattering. When applied to the cases of pair and triplet scatterings, our method produces results which are in agreement with those of Nickel and Krumhansl.

I. INTRODUCTION

The theory of disordered system has received a great deal of attention in recent years with the introduction of the coherent-potential approximation (CPA) by Soven.[1] This theory has been developed basically within the framework of multiple-scattering theory originally introduced by Lax.[2] It is a self-consistent method which serves as an interpolating scheme for the entire range of impurity concentrations and scattering strengths. In its original form, the single-site CPA is based on replacing the atomic potential at each lattice site by an undetermined coherent potential, the composition-independent off-diagonal terms in the Hamiltonian remaining unchanged. The self-consistency condition is introduced by requiring that the coherent potential, when placed at each lattice site of the ordered lattice, will reproduce all the properties of the actual crystal. Although the single-site CPA is exact to only first order in impurity concentration x, it nevertheless gives results better than any other methods which are also accurate to order of x simply because it includes not only all terms of first order in x, but also terms of higher order in x which are independent of z^{-1}, where z is the number of nearest neighbors.[3] The CPA theory has been widely used to study the static and dynamic properties of disordered alloys.[4,5] Comparison with exact numerical calculations has, however, shown, in particular, that the CPA fails to properly describe the impurity bands of disordered alloys.[6] The original CPA which is a single-site approximation neglects the effects due to formation of clusters and is restricted to alloys with composition-independent off-diagonal elements. Recently some attempts have been made to eliminate these shortcomings of the original CPA theory.

Cyrot-Lackmann and Ducastelle (CLD)[7] have extended the single-site CPA to take into account the pairing effects. They have concluded that their